Theory of the Interband Ferromagnetic Kerr Effect in Nickel*

BERNARD R. COOPER†
Division of Engineering and Applied Physics, Harvard University, Cambridge, Massachusetts
and
General Electric Research Laboratory, Schenectady, New York

(Received 2 April 1965)

A detailed discussion is given of the way in which the experimentally observed structure in the ferromagnetic Kerr effect (FKE) for nickel can be attributed to optical transitions involving the d and s bands near the Fermi surface. Absolute calculations are presented for $\epsilon_m^{(1)}$, the absorptive part of the off-diagonal element of the dielectric-constant tensor measured by the FKE, for models based on those recently proposed by Ehrenreich, Philipp, and Olechna and by Phillips and Mattheiss for the band structure of ferromagnetic nickel. For both models, the peak in $\epsilon_m^{(1)}$ is associated with transitions involving $\downarrow$ (minority-electron) spin bands. The results for the two models are compared with experiment, and this comparison is used to discuss their relative merit. Besides serving as a check on the validity of models for the band structure of ferromagnetic nickel developed from other experimental information, the FKE itself can be used as a tool for developing such models. A brief discussion of Models 3A and 3B previously developed on this basis is given. We call attention to the "step" expected at the onset of the contribution of the $\uparrow$ (majority-electron) bands to the FKE structure. Experimental observation of such structure in addition to the peak already associated with $\downarrow$-band transitions would serve to determine the d-band exchange splitting.

1. INTRODUCTION

THE use of the experimentally observed structure in the ferromagnetic Kerr effect (FKE) in understanding the electronic structure of ferromagnetic nickel has been discussed previously in two brief communications.[1,2] (Hereinafter, Refs. 1 and 2 are referred to as I and II, respectively.) In I and II, the observed low-frequency structure[3–6] was attributed to optical transitions involving the d and s bands near the Fermi surface. In I, the use of the FKE was discussed as a check on the validity of models for the band structure of ferromagnetic nickel[7–9] developed from other experimental information, while in II the use of the FKE itself as a tool for developing such models was discussed. The purpose of the present paper is to give a more complete account of the theory and calculations on which the discussion of I and II were based. This should help to emphasize the important information about the electronic structure of ferromagnetic metals to be gained from study of the FKE. We call attention to the "step" expected at the onset of the contribution of the $\uparrow$ (majority-electron) bands to the FKE structure.[2] Experimental observation of such structure in addition to the peak already associated with $\downarrow$-band transitions would serve to determine the exchange splitting.

The FKE is described by off-diagonal components ($\epsilon_m = \epsilon_m^{(1)} + i\epsilon_m^{(2)}$) of the dielectric constant tensor. It results from the effect of the spin-orbit interaction on the electronic wave functions and the unequal occupation of corresponding energy levels for $\uparrow$- and $\downarrow$-spin electrons.[10,11] In the present paper, we will give a detailed discussion as to how low-frequency structure in $\epsilon_m^{(1)}$, the absorptive part of ϵ_m, can arise for Models 1 and 2 of I; and we see how the result of absolute calculations compares to the experimental structure[12] shown in Fig. 1. A brief discussion of models 3A and 3B of II based on the detailed treatments of Models 1 and 2 is given. In the course of this discussion, a numerical error in II is corrected.

The picture we adopt for the physical basis of the FKE is that of Kittel[10] and Argyres.[11] We consider the situation where the electronic structure of Ni is described by spin-$\uparrow$ and spin-$\downarrow$ bands split by some sort of exchange or correlation energy. Then the Hamiltonian describing the situation for the FKE consists of three terms.

$$\mathcal{H} = \mathcal{H}_0 + \mathcal{H}_{s.o.} + \mathcal{H}_{opt}, \quad (1)$$

* Work at Harvard University supported by the U. S. Advanced Research Projects Agency and Office of Aerospace Research.

† Present address: General Electric Research Laboratory, Schenectady, New York.

[1] B. R. Cooper and H. Ehrenreich, Solid State Commun. **2**, 171 (1964). (Referred to as I.)

[2] B. R. Cooper, H. Ehrenreich, and L. Hodges, in Proceedings of the International Conference on Magnetism, Nottingham, England, September 1964 (to be published). (Referred to as II.)

[3] G. S. Krinchik and R. D. Nuralieva, Zh. Eksperim. i. Teor. Fiz. **36**, 1022 (1959) [English transl.: Soviet Phys.—JETP **9**, 724 (1959)].

[4] G. S. Krinchik, J. Appl. Phys. **35**, 1089 (1964).

[5] G. S. Krinchik and G. M. Nurmukhamedov, Zh. Eksperim. i. Teor. Fiz. **48**, 34 (1965) [English transl.: Soviet Phys.—JETP **21**, 22 (1965)].

[6] D. H. Martin, S. Doniach, and K. J. Neal, Phys. Letters **9**, 224 (1964).

[7] H. Ehrenreich, H. R. Philipp, and D. J. Olechna, Phys. Rev. **131**, 2469 (1963). (Referred to as EPO in the text.)

[8] J. C. Phillips and L. F. Mattheiss, Phys. Rev. Letters **11**, 556 (1963).

[9] J. C. Phillips, Phys. Rev. **133**, A1020 (1964).

[10] C. Kittel, Phys. Rev. **83**, 208(A) (1951).

[11] P. N. Argyres, Phys. Rev. **97**, 334 (1955).

[12] The data of Krinchik shown is that of Ref. 5. Two sets of data for ϵ_m of nickel, corresponding to different values of the ordinary optical constants, are given in Ref. 5. The data shown in Fig. 1 are those with amplitude of the main peak in $\epsilon_m^{(1)}$ more closely resembling that of Martin, Doniach, and Neal, Ref. 6. The other set of data in Ref. 5 has a peak value of $\epsilon_m^{(1)}$ equal to approximately -6.5, and the splitting of the main peak is less pronounced. The earlier data of Krinchik and co-workers given in Refs. 3 and 4 had very large uncertainties for frequencies below that of the main peak and had no indication of any splitting of the main peak.

where

$$\mathcal{H}_0=(1/2m)p^2+V(r), \tag{2a}$$

$$\mathcal{H}_{s.o.}=(1/2m^2c^2)[\nabla V\times\mathbf{p}]\cdot\mathbf{S}, \tag{2b}$$

$$\mathcal{H}_{opt}=(e/mc)\mathbf{A}\cdot\mathbf{p}. \tag{2c}$$

Here $\mathcal{H}_0$ is the usual one-electron Hamiltonian in the band approximation, whose eigenfunctions are the Bloch functions (orbital part),

$$\psi_{nk}=u_{nk}e^{i\mathbf{k}\cdot\mathbf{r}}\equiv|n,\mathbf{k}\rangle,$$

times spinor, α or β, for $\uparrow$- or $\downarrow$-spin electrons, respectively. $\mathcal{H}_{s.o.}$ is the spin-orbit interaction, while $\mathcal{H}_{opt}$ gives the interaction between the electronic system and an electromagnetic field. The FKE is one experimental manifestation of the off-diagonal elements of the dielectric constant tensor that arise because the Bloch functions between which the optical interaction (2c) causes transitions are modified by the spin-orbit coupling (2b). Argyres derived the expression for the off-diagonal elements of the dielectric constant for cubic crystals with nondegenerate bands using time-dependent perturbation theory. It is perhaps more illuminating to formulate the problem starting from the random-phase-approximation expression for the dielectric constant,[13,14] neglecting broadening and temperature effects,

$$\hat{\epsilon}=\hat{\epsilon}_1+i\hat{\epsilon}_2, \tag{3}$$

where

$$\hat{\epsilon}_1=\left(1-\frac{4\pi e^2N}{mV\omega^2}\right)\hat{1}-\frac{he^2}{m^2\pi^2\omega^2}\sum_\sigma\sum_{Et>E_F,En<E_F}P\int d\mathbf{k}\times\frac{\omega_{tn}(n\mathbf{k}|\mathbf{p}|t\mathbf{k})_\sigma(t\mathbf{k}|\mathbf{p}|n\mathbf{k})_\sigma}{\hbar^2(\omega^2-\omega_{tn}^2)} \tag{4}$$

and

$$\hat{\epsilon}_2=\frac{e^2}{2\pi m^2\omega^2\hbar}\sum_\sigma\sum_{Et>E_F,En<E_F}\int d\mathbf{k}(n\mathbf{k}|\mathbf{p}|t\mathbf{k})_\sigma\times(t\mathbf{k}|p|n\mathbf{k})_\sigma\delta(\omega-\omega_{tn}). \tag{5}$$

Here P denotes principal part of the integral, σ denotes the spin, and we use the notation $u_{nk}\equiv|n,\mathbf{k}\rangle$.

When $|n\mathbf{k})$ are given by the eigenfunctions of $\mathcal{H}_0$, then ϵ_1 and ϵ_2 are the real and imaginary parts of the ordinary dielectric constant which gives the ordinary optical absorption and has only equal diagonal elements for a cubic material. The off-diagonal elements of the dielectric constant tensor arise from the first-order perturbation on the $|n,\mathbf{k})$ caused by $\mathcal{H}_{s.o.}$ of (2b). (Within the approximation of complete orbital quenching, there is no change in the band energies to first order in $\mathcal{H}_{s.o.}$.) Since $\mathcal{H}_{s.o.}$ is an imaginary operator, the modification in $\hat{\epsilon}_1$ leads to the imaginary part of the off-diagonal elements of the dielectric constant, while the modification in $\hat{\epsilon}_2$ leads to the real part. (We use the notation $\hat{\epsilon}_m$ for the change in the dielectric constant due to the spin-orbit effects.) Thus the real part of the off-diagonal elements of the dielectric constant is the absorptive part. It is a straightforward procedure to show that

$$\epsilon_1{}^{ij}\text{ (first order in s.o.)}=i(\epsilon_{m\uparrow}{}^{ij(2)}+\epsilon_{m\downarrow}{}^{ij(2)}), \tag{6}$$

$$i\epsilon_{m\sigma}{}^{ij(2)}=(\pm)\frac{ihe^2}{m^2\pi^2\omega^2}\sum_{Et>E_F,En<E_F}P\int d\mathbf{k}\frac{\omega_{tn\sigma}Q_{tn\sigma}{}^{ij}}{(\omega^2-\omega_{tn\sigma}{}^2)}, \tag{7}$$

where the plus sign is for $\uparrow$ spin and the minus sign for $\downarrow$ spin, and

$$Q_{tn\sigma}{}^{ij}=\frac{i}{2\hbar^2}\sum_l{}'\left[\frac{\langle l|0_z|n\rangle_\sigma{}^*}{\omega_{nl\sigma}}(l|p_i|t)_\sigma(t|p_j|n)_\sigma+\frac{\langle l|0_z|n\rangle_\sigma(n|p_i|t)_\sigma(t|p_j|l)_\sigma}{\omega_{nl\sigma}}+\frac{\langle l|0_z|t\rangle_\sigma(n|p_i|l)_\sigma(t|p_j|n)_\sigma}{\omega_{tl\sigma}}+\frac{\langle l|0_z|t\rangle_\sigma{}^*(n|p_i|t)_\sigma(l|p_j|n)_\sigma}{\omega_{tl\sigma}}\right], \tag{8}$$

with

$$0\equiv[1/(2m^2c^2)](\nabla V\times\mathbf{p}), \tag{9}$$

where the matrix elements in (8) are for the zero-order wave functions, so that $Q_{tn\sigma}{}^{ij}$ is real. Since the spin-orbit interaction has the lattice periodicity, all the ma-

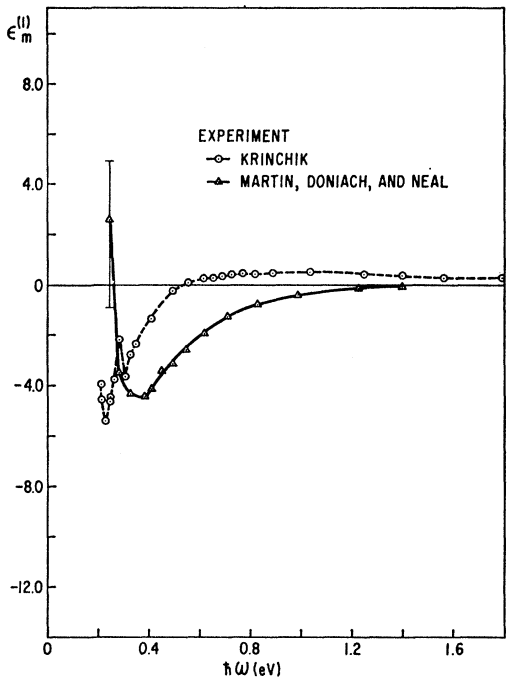

FIG. 1. Experimental spectral dependence of $\epsilon_m{}^{(1)}$ for nickel. The data of Krinchik shown is that of Ref. 5.

[13] H. Ehrenreich and M. H. Cohen, Phys. Rev. **115**, 786 (1959).
[14] S. L. Adler, Phys. Rev. **126**, 413 (1962).

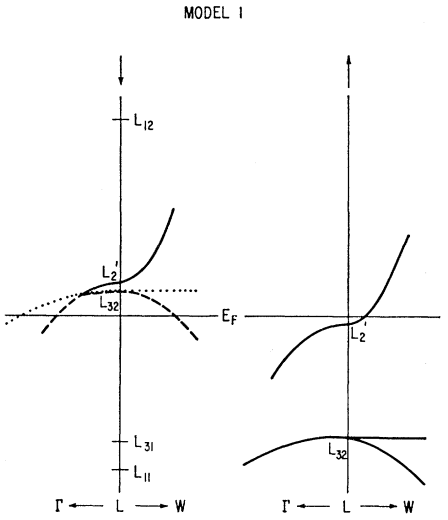

FIG. 2. Band structure near L for Model 1.

trix elements in Eq. (8) are for a given $\mathbf{k}$; and $Q_{tn\sigma}{}^{ij}$ is a function of $\mathbf{k}$. It should be noted that (7) differs from the expression obtained from Eq. (18) of Ref. 11 by a factor $\omega_{tn\sigma}/\omega$. This occurs because the procedure used in Ref. 11 is equivalent to improperly linearizing the Liouville equation used in obtaining the dielectric constant tensor.

Similarly, the absorptive part of the off-diagonal elements of the dielectric constant tensor is given by

$$i\epsilon_2{}^{ij} \text{ (first order in s.o.)} = -(\epsilon_{m\uparrow}{}^{ij(1)} + \epsilon_{m\downarrow}{}^{ij(1)}), \quad (10)$$

with

$$\epsilon_{m\sigma}{}^{ij(1)} = -(\pm)\frac{e^2h}{2\pi m^2\omega^2} \sum_{E_t>E_F, E_n<E_F} \int d\mathbf{k} \times Q_{tn\sigma}{}^{ij}\delta(\omega-\omega_{tn\sigma}), \quad (11)$$

where the plus sign is for ↑ spin and the minus sign for ↓ spin. This agrees with the result obtained from Eq. (18) of Ref. 11. Because of the opposite signs of $\epsilon_{m\uparrow}$ and $\epsilon_{m\downarrow}$, there is zero net off-diagonal contribution to the dielectric constant for a nonmagnetic material. There is a net contribution for a ferromagnetic material because of the shift in energy of ↓-spin bands relative to ↑-spin bands as well as any difference in corresponding wave functions for ↑- and ↓-spin bands.

It is clear from the preceding discussion that the Kramers-Kronig relationship for $\epsilon_m{}^{(1)}$ and $\epsilon_m{}^{(2)}$ is the same as that for ϵ_1 and ϵ_2, with $\epsilon_1 \rightarrow \epsilon_m{}^{(2)}$ and $\epsilon_2 \rightarrow \epsilon_m{}^{(1)}$, i.e., the real and imaginary parts interchanged.

By use of the fact that $\langle l|0_z|n\rangle$ is imaginary and $(l|p_i|m)$ is real (which follows from time reversal and space-inversion symmetry) and Hermitian, it is easy to show that

$$Q_{tn\sigma}{}^{ji} = -Q_{tn\sigma}{}^{ij}. \quad (12)$$

Thus, $Q_{tn\sigma}$ and, consequently, $\epsilon_{m\sigma}{}^{ij(1)}$ and $\epsilon_{m\sigma}{}^{ij(2)}$ are antisymmetric tensors, so that the spin-orbit coupling to lowest order affects only the off-diagonal elements of the dielectric constant.

For a cubic crystal, the requirement that $\hat{\epsilon}_m$ be invariant under the 48 operators of the group 0_h simplifies the form[11] of $\hat{\epsilon}_m$. Taking the z axis as the direction of magnetization, only the xy components of $\hat{\epsilon}_m$ are nonvanishing, so that[15]

$$\hat{\epsilon} = \begin{bmatrix} \epsilon_1+i\epsilon_2 & -(\epsilon_m{}^{(1)}+i\epsilon_m{}^{(2)}) & 0 \\ (\epsilon_m{}^{(1)}+i\epsilon_m{}^{(2)}) & \epsilon_1+i\epsilon_2 & 0 \\ 0 & 0 & \epsilon_1+i\epsilon_2 \end{bmatrix}, \quad (13)$$

where $\epsilon_{m\sigma}{}^{(1)}$ is given by (11) suppressing the superscripts ij, with

$$Q_{tn\sigma} = \frac{i}{\hbar^2}\sum_l{}' \left[\frac{\langle l|0_{x_3}|n\rangle_\sigma{}^*(l|p_{x_1}|t)_\sigma(t|p_{x_2}|n)_\sigma}{\omega_{nl\sigma}} + \frac{\langle l|0_{x_3}|t\rangle_\sigma(n|p_{x_1}|l)_\sigma(t|p_{x_2}|n)_\sigma}{\omega_{tl\sigma}} \right]. \quad (14)$$

x_1, x_2, x_3 denote the cubic axes of the crystal.

In the present work, we will discuss to what extent the experimental structure in $\epsilon_m{}^{(1)}$ at about 0.3 eV (Fig. 1) can be associated with optical transitions involving the ↓-spin[16] d and s electrons near the Fermi surface for Models 1 and 2 of I. We will also discuss what additional structure may occur because of transitions involving ↑-spin electrons.

As discussed recently by Cooper, Ehrenreich, and Philipp,[17] for metals there are two ways in which sharp structure can occur in the ordinary optical absorption. Sharp optical structure may be associated with localized regions of k space surrounding critical points[18,19] in the joint density of states, or in metals with regions (not necessarily associated with critical points) where the location of the Fermi level is such that vertical interband transitions extending over a finite range of k space between a filled and an unfilled band suddenly become possible. The same two possibilities occur for the FKE. All the possibilities for the occurrence of sharp structure discussed in this paper are of the second type, that is, transitions become possible over a substantial part of the Brillouin zone for increases in photon energy of a few tenths of an electron volt. In the limited region of the Brillouin zone considered, it is permissible to assume $Q_{tn}(\mathbf{k})$ between a pair of bands to be constant when the transition is everywhere al-

[15] The notation $\epsilon_{m\uparrow}{}^{ij(1)}$, $\epsilon_{m\uparrow}{}^{ij(2)}$ follows that of Cooper and Ehrenreich. (Reference 1.) Unfortunately, the notation for the off-diagonal elements of the dielectric constant tensor varies. The relationship between the definitions for the pertinent references is indicated below: $\epsilon_m{}^{(1)} = \epsilon_2''$ (Ref. 6, Martin, Doniach, and Neal) $= \epsilon_2'$ (Refs. 4, 5 Krinchik), $\epsilon_m{}^{(2)} = \epsilon_2'$ (Ref. 6, Martin, Doniach, and Neal) $= \epsilon_1'$ (Refs. 4, 5 Krinchik).

[16] We take the majority electrons leading to a net magnetization to have ↑ spin.

[17] B. R. Cooper, H. Ehrenreich, and H. R. Philipp, Phys. Rev. **138**, A494 (1965).

[18] L. Van Hove, Phys. Rev. **89**, 1189 (1953).

[19] J. C. Phillips, J. Phys. Chem. Solids **12**, 208 (1960).

lowed. In the next two sections we will discuss how, with this approximation, structure occurs for Models 1 and 2 of I. In Sec. 4, we briefly discuss Models 3A and 3B of II. In the final section of the paper, we will discuss the result of the calculated values of $\epsilon_m^{(1)}$ for Models 1 and 2, their comparison to each other and to experiment.

2. CALCULATION OF $\epsilon_m^{(1)}$ FOR MODEL 1

In this section, we consider the lowest frequency interband structure in $\epsilon_m^{(1)}$ for the model of the band structure and Fermi surface of nickel suggested by Ehrenreich, Philipp, and Olechna,[7] which, following the notation of I, we refer to as Model 1. In this model, as in that of Phillips and Mattheiss[8,9] discussed below, the lowest frequency interband transitions are thought to occur near the point L where the Fermi level crosses several closely lying $\downarrow$ bands.

A. Calculation of $\epsilon_m^{(1)}$ in Terms of Band Parameters

The band structure near L for Model 1 is shown in Fig. 2. The optical transitions of interest for the $\downarrow$ bands occur between the filled portion of the lower band l (dashed curve) and the unfilled upper band u (dotted curve). In the absence of damping effects, the contribution to $\epsilon_m^{(1)}$ from the pair of bands is given by (11), for the case of a single pair of $\downarrow$ bands.

$$\epsilon_m^{(1)}=\frac{e^2h}{2\pi m^2\omega^2}\int_{El<E_F,Eu>E_F} d\mathbf{k}\delta(\omega_{ul}-\omega)Q_{ul}(\mathbf{k}). \quad (15)$$

The contribution to $\epsilon_m^{(1)}$ arising from transitions between the dashed and dotted $\downarrow$ curves in Fig. 2 can be found from (15) taking Q as the value at L. To simplify these calculations further, in calculating the shapes of the frequency dependence of $\epsilon_m^{(1)}$ we neglect the energy difference between $L_{32\downarrow}$ and $L_{2'\downarrow}$ and assume the dashed $\downarrow$ band to be parabolic with $m_{l\downarrow\downarrow}=m_{l\downarrow\downarrow}$ $(L_{2'})$ and[20] $m_{l\perp}=m_{\perp\downarrow}$ $(L_{321\text{m.}})$. (We use $\parallel$ and $\perp$ throughout to denote quantities which are appropriate, respectively, parallel and perpendicular to the L-Γ direction.) Also we take the dotted band as parabolic with $m_{u\downarrow\downarrow}=m_{\downarrow\downarrow}(L_{32})$ and $m_{u\perp}=m_{\perp\downarrow}$ $(L_{32\text{h.m.}})$, which we take equal to ∞ (well representing the results of the band calculations of Hanus[21]). Thus, we actually calculate the shape of the frequency dependence of $\epsilon_m^{(1)}$ for the model shown in Fig. 3. However, the angular dependence of Q is adjusted in a manner described subsequently to allow for the fact that optical transitions are forbidden between the dashed and dotted $\downarrow$ bands of Fig. 2 in the $\perp$ direction as one approaches L. As we shall now show, these considerations then completely determine the shape of

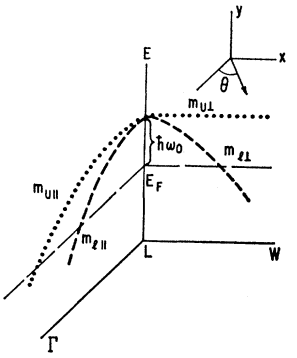

FIG. 3. Approximation to band structure near L used to calculate $\epsilon_m^{(1)}$ for Model 1.

the frequency dependence curves for the low-frequency $\downarrow$-band contribution to $\epsilon_m^{(1)}$.

To find the frequency dependence of $\epsilon_m^{(1)}$ from (15), we wish to evaluate the integral

$$Q\xi(\omega)\equiv\int_{El<E_F,Eu>E_F} d\mathbf{k}\delta(\omega_{ul}-\omega)Q_{ul}(\mathbf{k}), \quad (16)$$

where Q on the left-hand side is the magnitude of $Q_{ul}(\mathbf{k})$ connecting the two bands of interest evaluated at one of the points L in the Brillouin zone. For the model of Fig. 3, taking the zeros of $\mathbf{k}$ and energy at L and E_F, respectively,

$$\omega_u=\omega_0+(\hbar k_{\parallel}^2/2m_{u\parallel}), \quad (17a)$$

$$\omega_l=\omega_0+(\hbar k_{\parallel}^2/2m_{l\parallel})+(\hbar k_{\perp}^2/2m_{l\perp}). \quad (17b)$$

Defining

$$c_{u\parallel}=-(\hbar/2m_{u\parallel}), \quad (18a)$$

$$c_{l\parallel}=-(\hbar/2m_{l\parallel}), \quad c_{l\parallel}>c_{u\parallel}>0, \quad (18b)$$

$$c_{\parallel}=c_{l\parallel}-c_{u\parallel}>0, \quad (18c)$$

$$c_{l\perp}=-(\hbar/2m_{l\perp}), \quad (18d)$$

then

$$\omega_{ul}=c_{\parallel}k_{\parallel}^2+c_{l\perp}k_{\perp}^2; \quad (19)$$

and we can evaluate the integral of (16) using the transformation

$$k_x=(\omega_{ul}/c_{l\perp})^{1/2}\sin\theta\cos\varphi, \quad (20a)$$

$$k_y=(\omega_{ul}/c_{l\perp})^{1/2}\sin\theta\sin\varphi, \quad (20b)$$

$$k_{\parallel}=(\omega_{ul}/c_{l\parallel})^{1/2}\cos\theta, \quad (20c)$$

where here the x and y axes are any two axes at right angles orthogonal to the $\parallel$ direction, so that $k_{\perp}^2=k_x^2+k_y^2$. We allow for the fact that optical transitions are forbidden between the dashed and dotted $\downarrow$ bands of Fig. 2 in the $\perp$ direction as one approaches L by taking

$$Q_{ul}(\mathbf{k})=Q\cos\theta. \quad (21)$$

Then

$$\xi(\omega)=(\pi/c_{l\perp})(\omega/c_{l\parallel})^{1/2}[(\cos\theta_{\text{upper}})^2-(\cos\theta_{\text{lower}})^2]. \quad (22)$$

Here $\cos\theta_{\text{lower}}$ and $\cos\theta_{\text{upper}}$ are determined, respectively, from the conditions that $\omega_l<0$, $\omega_u>0$. The condition

[20] We use the abbreviation $L_{32\text{ l.m.}}$ and $L_{32\text{ h.m.}}$ to denote quantities pertaining to the light and heavy mass L_{32} levels, respectively.

[21] J. H. Hanus, MIT Solid State and Molecular Theory Group Quarterly Progress Report No. 44, 1962 (unpublished).

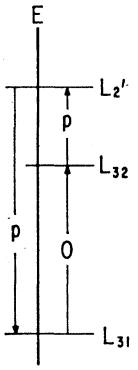

FIG. 4. Interactions giving rise to Q at L.

$\omega_l<0$ gives

$$\omega<\frac{c_{11}}{c_{l11}}\omega_0, \quad \cos\theta_{\text{lower}}=1, \tag{23a}$$

$$\frac{c_{11}}{c_{l11}}\omega_0<\omega<\omega_0, \quad \cos\theta_{\text{lower}}=\left(\frac{c_{11}}{c_{u11}}\right)^{1/2}\left(\frac{\omega_0-\omega}{\omega}\right)^{1/2}, \tag{23b}$$

$$\omega>\omega_0, \quad \cos\theta_{\text{lower}}=0. \tag{23c}$$

The frequency $(c_{11}/c_{l11})\omega_0$ is the value of ω_{ul} when the lower band first cuts the Fermi energy and transitions become allowed. This occurs in the $\parallel$ direction. As the frequency increases, transitions are possible for a part of the region of the Brillouin zone surrounding L which increases in angle toward the $\perp$ direction until, at ω_0, transitions are possible for the entire region of the Brillouin zone surrounding L.

The condition $\omega_u>0$ gives

$$\omega<(c_{11}\omega_0)/c_{u11}, \quad \cos\theta_{\text{upper}}=1, \tag{24a}$$

$$\omega>(c_{11}\omega_0)/c_{u11}, \quad \cos\theta_{\text{upper}}=((c_{11}/c_{u11})(\omega_0/\omega))^{1/2} \tag{24b}$$

For the case at hand, $c_{11}/c_{u11}>1$, so that (24) simply expresses the fact that, as the frequency increases from ω_0, at $\omega=(c_{11}\omega_0)/c_{u11}$ the upper band cuts the Fermi surface in the $\parallel$ direction, and thus transitions become forbidden in that direction. As ω increases, the part of the Brillouin zone for which transitions are forbidden spreads toward the $\perp$ direction.

By combining (22), (23), and (24), we obtain the frequency dependence of $Q\xi(\omega)$ and hence, from (15), that of $\epsilon_m^{(1)}$.

B. Band Parameters Used in Calculations

We now indicate how we obtain the various band masses and the value of $\hbar\omega_0$ for the model described in Sec. 2.A above.

The value of $\hbar\omega_0$ is taken as $E_\downarrow(L_{32})-E_F$ for the band structure of EPO.[7] This gives

$$\hbar\omega_0=0.24 \text{ eV}. \tag{25}$$

As indicated above, we identify the various effective masses for the model of Fig. 3 with the band masses as follows:

$$m_{l11}=m_{11\downarrow}(L_{2'}), \tag{26}$$

$$m_{u11}=m_{11\downarrow}(L_{32}), \tag{27}$$

$$m_{l\perp}=m_{\perp\downarrow}(L_{32\text{ l.m.}}). \tag{28}$$

The value used for $m_{11\downarrow}(L_{2'})$ is estimated using $\mathbf{k}\cdot\mathbf{p}$ perturbation theory, as well as the experimental transverse and longitudinal effective mass values from de Haas–von Alphen measurements[22] [$m_{\perp\uparrow}(L_{2'})=0.26m_0$ and $m_{11\uparrow}(L_{2'})=-0.65m_0$] and band gaps given by EPO.[7]

From $\mathbf{k}\cdot\mathbf{p}$ perturbation theory,

$$\frac{m}{m_{\perp\uparrow}(L_{2'})}=1+\frac{2}{m}\sum_{j=L_3}\frac{|(L_j|p_\perp|L_{2'})_\uparrow|^2}{E_\uparrow(L_{2'})-E_\uparrow(L_j)}, \tag{29}$$

$$\frac{m}{m_{11\uparrow}(L_{2'})}=1+\frac{2}{m}\sum_{j=L_1}\frac{|(L_j|p_{11}|L_{2'})_\uparrow|^2}{E_\uparrow(L_{2'})-E_\uparrow(L_j)}. \tag{30}$$

It is assumed (i) that all $\mathbf{p}$ matrix elements between s and d bands at L have the same magnitude and (ii) that corresponding $\mathbf{p}$ matrix elements are the same for $\uparrow$- and $\downarrow$-spin bands. Then using the experimental value of $m_{\perp\uparrow}(L_{2'})$ and $\uparrow$-band separations at L given by EPO[7] in Eq. (29) with assumption (i) yields

$$E_p=1.5 \text{ eV}, \tag{31}$$

where

$$\begin{aligned}E_p&\equiv(2/m)|(L_{2'}|p_\perp|L_{32\text{ h.m.}})|^2\\&\approx(2/m)|(L_{2'}|p_\perp|L_{32\text{ l.m.}})|^2\\&\approx(2/m)|(L_{2'}|p_\perp|L_{31})|^2\approx(2/m)|(L_{2'}|p_{11}|L_{11})|^2.\end{aligned} \tag{32}$$

From (30), using this value for E_p, the experimental value of $m_{11\uparrow}(L_{2'})$, and $\uparrow$-band separations at L from EPO,[7] we then find

$$(2/m)|(L_{12}|p_{11}|L_{2'})|^2=17.5 \text{ eV}. \tag{33}$$

Then, following assumption (ii), the values of matrix elements given in (31) and (33) can be used in (30) together with the EPO[7] $\downarrow$-band separations to give

$$m_{l11}=m_{11\downarrow}(L_{2'})=-0.83m_0. \tag{34}$$

The value of E_p given in (32) will also be used in the following section in estimating the magnitude of $Q_{ul}(L)$.

The values of $m_{11\downarrow}(L_{32})$ and $m_{\perp\downarrow}(L_{32\text{ l.m.}})$ cannot be obtained from $\mathbf{k}\cdot\mathbf{p}$ perturbation theory and are therefore obtained by fitting the corresponding band curvatures for Hanus'[21] calculations. This gives

$$m_{u11}=m_{11\downarrow}(L_{32})=-2.5m_0, \tag{35a}$$

$$m_{l\perp}=m_{\perp\downarrow}(L_{32\text{ l.m.}})=-0.73m_0. \tag{35b}$$

C. Evaluation of Q_{ul} at L

The constant value of Q used in our calculations is evaluated from the wave functions at L. This pro-

[22] A. S. Joseph and A. C. Thorsen, Phys. Rev. Letters **11**, 554 (1963).

cedure is based on considering the situation for the ↓ bands of Fig. 2 in the || direction in the region where transitions between the dashed and dotted bands are allowed. Then the dashed band corresponds to the $L_{2'}$ band and the dotted band to the lower of the two sheets going through L_{32}. Thus we evaluate Q on the basis of transitions between the $L_{2'}$ wave function and the lower of the two L_{32} wave functions when the L_{32} degeneracy is removed by spin-orbit interaction. The nonzero value of Q so obtained depends on the mixing of the L_{32} wave function with the nearest lying wave functions with which such mixing is allowed, the two degenerate L_{31} levels. The interactions giving Q at L are indicated in Fig. 4. We consider the spin-orbit mixing in the tight-binding approximation.[23]

If we take the atomic functions corresponding to the fivefold degenerate $3d$ level of the isolated atom,

$$\begin{aligned}
\varphi_1&=(15/4\pi)^{1/2}x_1x_2f(r)/r^2,\\
\varphi_2&=(15/4\pi)^{1/2}x_2x_3f(r)/r^2,\\
\varphi_3&=(15/4\pi)^{1/2}x_1x_3f(r)/r^2,\\
\varphi_4&=(15/16\pi)^{1/2}(x_1^2-x_2^2)f(r)/r^2,\\
\varphi_5&=(5/16\pi)^{1/2}(3x_3^2-r^2)f(r)/r^2,
\end{aligned} \tag{36}$$

and define the linear combinations

$$\psi_{nk}=\sum_{R_i}\exp(i\mathbf{R}_i\cdot\mathbf{k})\varphi_n(\mathbf{r}-\mathbf{R}_i)\quad n=1,\cdots,5, \tag{37}$$

then the d wave functions at L for the tight binding calculation are linear combinations of the ψ_{nk} whose coefficients are readily obtained from Fletcher's work.[23,24]

Brooks[25] demonstrated that for ψ_{nk} of the form (37),

$$\begin{aligned}\langle i|0_{x_3}S_{x_3}|j\rangle&=\tfrac{1}{2}\hbar\langle i|0_{x_3}|j\rangle\approx A(i|l_{x_3}s_{x_3}|j)\\&=\tfrac{1}{2}A(i|l_{x_3}|j),\end{aligned} \tag{38}$$

where l_{x_3} and s_{x_3} are the orbital and spin angular momenta in units of $\hbar$, and $(i|l_{x_3}|j)$ is the matrix element of l_{x_3} between the atomic wave functions φ_i and φ_j. A is the ordinary spin-orbit parameter for free atoms[26] and has the value

$$A=633.3\text{ cm}^{-1} \tag{39}$$

for nickel.

We are interested in evaluating Q corresponding to optical transitions from the lower of the two spin-orbit split L_{32} levels to the $L_{2'}$ level. The pertinent spin-orbit mixing is between the correct zero-order L_{32} wave function and the L_{31} wave functions. The zero-order L_{32} functions are (with energy relative to the unperturbed L_{32} level)

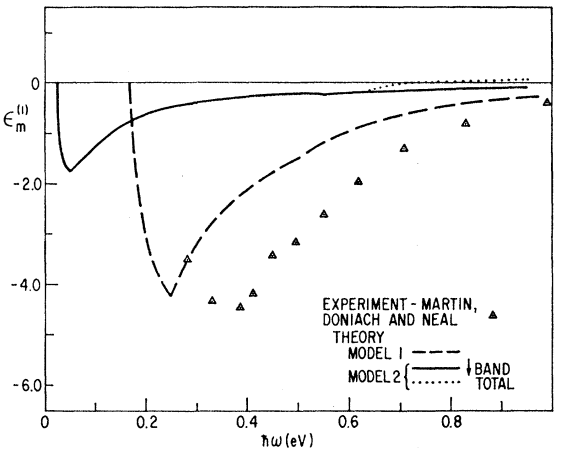

FIG. 5. Spectral dependence of $\epsilon_m^{(1)}$: Theoretical curves for Models 1 and 2 described in the text are shown as well as the experimental values of Martin, Doniach, and Neal.

$$\varphi_{L_{32\alpha}}=(1/\sqrt{2})(\varphi_{L_{32\text{ l.m.}}}-i\varphi_{L_{32\text{ h.m.}}}),\quad E=0.40(A/2), \tag{40a}$$

$$\varphi_{L_{32\beta}}=(1/\sqrt{2})(\varphi_{L_{32\text{ l.m.}}}+i\varphi_{L_{32\text{ h.m.}}}),\quad E=-0.40(A/2), \tag{40b}$$

where we note, incidentally, that this indicates a spin-orbit splitting of the L_{32} band $=0.40A=0.03$ eV.

The question arises as to whether there is a contribution to the off-diagonal elements of the dielectric constant tensor to zero order in the spin-orbit coupling for degenerate bands split by spin-orbit coupling as in (40). If there is, the spin-orbit mixing with the L_{31} levels need not be considered. This question can be answered by substituting the wave functions of either (40a) or (40b) for n in the general expression for ϵ_2, Eq. (5). It is a straightforward matter to show that for cubic symmetry this gives zero contribution to the off-diagonal elements of the dielectric constant tensor. Thus, as already indicated, we have to look to the spin-orbit mixing of the $L_{32\beta}$ wave function with the L_{31} wave functions to obtain a nonvanishing value for Q.

The present situation differs slightly from that discussed in Sec. 2.A in connection with Eqs. (8) and (11) in that the wave function $|n)$ is no longer real but of the form given by (40b). This introduces a small modification in the form of Q as given by (14) so that[24]

$$\begin{aligned}Q(L)=-\frac{1}{\hbar[E(L_{32})-E(L_{31})]}\,\mathrm{Im}[&\langle L_{31\alpha}|0_{x_3}|L_{32\beta}\rangle\\&\times(L_{2'}|p_{x_1}|L_{31\alpha})(L_{32\beta}|p_{x_2}|L_{2'})\\&+\text{same with }L_{31\alpha}\rightarrow L_{31\beta}],\end{aligned} \tag{41}$$

where the quantities involved are for the ↓ bands.

Then using the approximation of (38) together with

[23] G. C. Fletcher, Proc. Phys. Soc. (London) **65**, 192 (1952).

[24] A more detailed discussion of this point can be found in General Electric Research Laboratory Report No. 65-R.L.-3918E (unpublished) by Bernard R. Cooper. This is available upon request.

[25] H. Brooks, Phys. Rev. **58**, 909 (1940).

[26] S. Goudsmit, Phys. Rev. **31**, 946 (1928).

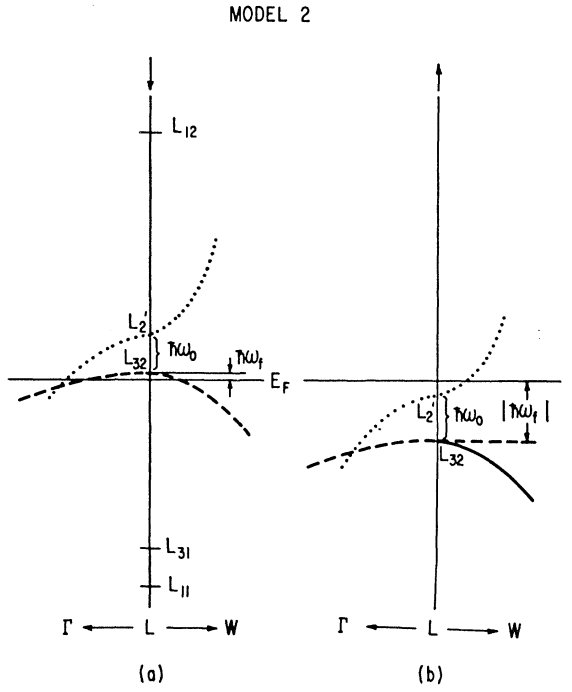

FIG. 6. Band structure near L for Model 2.

(40) and the correct linear combinations of the ψ_{nk} for the d wave functions at L gives

$$Q(L)=\{A/2\hbar^2[E(L_{32})-E(L_{31})]\}\times[1.34(L_{2'}|p_{x_1}|L_{31\alpha})(L_{32\,\text{l.m.}}|p_{x_2}|L_{2'})+0.29(L_{2'}|p_{x_1}|L_{31\beta})(L_{32\,\text{h.m.}}|p_{x_2}|L_{2'})]. \quad (42)$$

Exactly the same expression would be obtained by considering transitions involving $L_{32\alpha}$ rather than $L_{32\beta}$.

With the approximation that the momentum matrix elements at L between all s and d wave functions are equal in magnitude, we have

$$\frac{2}{m}(L_{2'}|p_{x_1}|L_{31})(L_{32}|p_{x_2}|L_{2'}) \leq \frac{2}{m}|(L_{2'}|p_1|L_{32})|^2=E_p. \quad (43)$$

So that replacing each of the products of momentum matrix elements of this form in (42) by E_p gives an upper limit on $Q(L)$ within the framework of the tight-binding treatment for the d-band spin-orbit mixing. Although an upper limit, this value is expected to represent a reasonable estimate. This procedure then gives the value of Q used in the numerical calculations.

$$Q(L)\approx\{1.63/4\hbar^2[E(L_{32})-E(L_{31})]\}AmE_p. \quad (44)$$

This same expression applies for Model 2 discussed below for both ↓ and ↑ bands. Since one usually assumes that the splitting within the d-band complex remains constant, the only change in $Q(L)$ for different models within the present context comes from changes in E_p.

For Model 1, (44) gives

$$Q_\downarrow(L)=2.9(10^{13})\ \text{cm}^{-2}. \quad (45)$$

Q as determined in (45) is guaranteed to be real; however, its sign is not determined by the procedure used here.

D. Numerical Results and Comparison with Experiment

The spectral variation of $\epsilon_m^{(1)}$ is evaluated for the ↓-band contribution for Model 1 using Eqs. (15), (16), and (22), where the pertinent numerical values of parameters are given in Sec. 2.B and Eq. (45). An additional factor of 4 is included in the evaluation of $\epsilon_m^{(1)}$ to account for the fact that there are 4 L's in the Brillouin zone whose neighborhoods contribute. The calculated values of $\epsilon_m^{(1)}$ for Model 1 are compared to the experimental values of Martin, Doniach, and Neal[6] in Fig. 5. Since the sign of $\epsilon_m^{(1)}$ is not determined by the present calculation, it is chosen to agree with experiment. The theoretical values of $\epsilon_m^{(1)}$ differ from those of I because of improvements in the method of estimating Q and certain of the band curvatures. The theoretical curve gives generally good agreement with the experimentally observed structure, particularly considering the neglect of broadening effects.

3. CALCULATION OF $\epsilon_m^{(1)}$ FOR MODEL 2

Model 2 is meant to yield, insofar as is practical, the same results for the FKE as would be obtained for the model of Phillips and Mattheiss.[8,9] Insofar as is possible, band parameters have been given the same values as in that model; however, we have made additional approximations and assumptions. In the following discussion, the quantities taken directly from Refs. 8 and 9 are indicated.

A. Band Parameters for Model 2

The band structure near L for Model 2 is shown in Fig. 6. The band separations at L and the sources for the values are as follows:

	↓ bands	↑ bands
$E(L_{12})-E(L_{2'})$	6.93 eV (Ref. 21)	6.93 eV (Ref. 21)
$E(L_{2'})-E(L_{32})$	0.3 eV [Eq. (18) of Ref. 8]	0.5 eV [Eq. (14) of Ref. 8]
$E(L_{32})-E_F$	0.05 eV [Eq. (16) of Ref. 8]	
$E_F-E(L_{2'})$		0.13 eV [Eq. (15) of Ref. 8]
$E(L_{32})-E(L_{31})$	2.16 eV (Ref. 21)	2.16 eV (Ref. 21)
$E(L_{31})-E(L_{11})$	2.39 eV (Ref. 21)	2.39 eV (Ref. 21).

(46)

This gives the values for the energy differences $\hbar\omega_f$ indicated in Fig. 6.

$$\begin{aligned} &\qquad\qquad \downarrow \text{bands} \qquad \uparrow \text{bands} \\ &\hbar\omega_0 \equiv E(L_{2'}) - E(L_{32}) = 0.3 \text{ eV} \qquad 0.5 \text{ eV} \\ &\hbar\omega_f \equiv E(L_{32}) - E_f \quad = 0.05 \text{ eV} \qquad -0.63 \text{ eV}. \end{aligned} \tag{47}$$

E_p and Q are determined by exactly the same procedure as described in Sec. 2 for Model 1. This gives

$$E_p = 0.6 \text{ eV}, \tag{48}$$

$$Q = 1.2(10^{13}) \text{ cm}^{-2}. \tag{49}$$

These values apply for both $\downarrow$ and $\uparrow$ bands. We should note that Phillips and Mattheiss[8] determine values for E_p by a method different than the one used here. Their method is based on considering the variation of E_p with $\hbar\omega_0$ for several different band calculations. Their value for E_p, and hence Q, would be substantially larger than that quoted here, probably by a factor of 2 or 3.

Just as for Model 1, $m_{11\uparrow}(L_{2'})$ and $m_{1\uparrow}(L_{2'})$ are taken as equal to the experimental de Haas–van Alphen values,[22]

$$m_{1\uparrow}(L_{2'}) = 0.26 m_0, \tag{50a}$$

$$m_{11\uparrow}(L_{2'}) = -0.65 m_0. \tag{50b}$$

By the same procedure as that described in Sec. 2 for Model 1 using $\mathbf{k}\cdot\mathbf{p}$ perturbation theory, we obtain

$$m_{1\downarrow}(L_{2'}) = 0.18 m_0, \tag{51a}$$

$$m_{11\downarrow}(L_{2'}) = -0.65 m_0. \tag{51b}$$

From Eq. (6.12) of Ref. 9,

$$m_{11\downarrow}(L_{32}) = m_{11\uparrow}(L_{32}) = -3 m_0. \tag{52}$$

By fitting the bands of Hanus,[21]

$$m_{1\downarrow}(L_{32\ \text{l.m.}}) = m_{1\uparrow}(L_{32\ \text{l.m.}}) = -0.73 m_0. \tag{53}$$

B. Structure in $\epsilon_m^{(1)}$ for Model 2 $\downarrow$ Bands

The optical transitions of interest for the $\downarrow$ bands of Model 2 occur between the dashed and dotted bands of Fig. 6 when the dashed band is below and the dotted band above the Fermi energy. Just as for Model 1, for the purpose of calculating the magneto-optical structure, we approximate the band shapes as being parabolic. With the zero of $\mathbf{k}$ and energy at L and E_F, respectively,

$$\omega_u = \omega_0 + \omega_f + c_{u1}k_1^2 - c_{u11}k_{11}^2, \tag{54}$$

where

$$c_{u1} = \hbar/2m_{u1} > 0, \quad c_{u11} = -\hbar/2m_{u11} > 0 \tag{55}$$

and

$$m_{u1} = m_{1\downarrow}(L_{2'}), \quad m_{u11} = m_{11\downarrow}(L_{2'}), \tag{56}$$

$$\omega_l = \omega_f - c_{l1}k_1^2 - c_{l11}k_{11}^2, \tag{57}$$

where

$$c_{l1} = -\hbar/2m_{l1} > 0, \quad c_{l11} = -\hbar/2m_{l11} > 0 \tag{58}$$

and

$$m_{l1} = m_{1\downarrow}(L_{32\ \text{l.m.}}), \quad m_{l11} = m_{11\downarrow}(L_{32}). \tag{59}$$

Then

$$\omega_{ul} = \omega_0 + c_1 k_1^2 - c_{11}k_{11}^2, \tag{60}$$

with

$$c_1 = c_{u1} + c_{l1}, \tag{61a}$$

$$c_{11} = c_{u11} - c_{l11}, \tag{61b}$$

s that $c_1 > c_{11} > 0$.

We obtain $\epsilon_m^{(1)}$ from (15) taking $Q_{ul}(\mathbf{k})$ equal to the constant value given by (49) since the transitions are allowed in all directions around L:

$$\epsilon_m^{(1)} = [(e^2\hbar Q)/(2\pi m^2\omega^2)]\eta(\omega), \tag{62}$$

where

$$\eta(\omega) = \int_{E_l < E_F, E_u > E_F} d\mathbf{k}\,\delta(\omega_{ul} - \omega). \tag{63}$$

For $\hbar\omega < \hbar\omega_0$, it is a straightforward procedure to evaluate $\eta(\omega)$, using a transformation similar to that of Eq. (20) but of a form to take account of the fact that the energy difference surfaces are hyperboloids of two sheets.[24] This gives

$$\eta(\omega) = (2\pi/c_1)[(\omega_0 - \omega)/c_{11}]^{1/2} \times (\cosh v_{\text{upper}} - \cosh v_{\text{lower}}). \tag{64}$$

Here $\cosh v_{\text{upper}}$ is determined by the condition $\omega_u > 0$.

$$\cosh v_{\text{upper}} = \left\{ \frac{\omega_0 + \omega_f - (c_{u1}/c_1)(\omega_0 - \omega)}{[(c_{u11}/c_{11}) - (c_{u1}/c_1)](\omega_0 - \omega)} \right\}^{1/2}. \tag{65}$$

The absolute lower bound on $\cosh v$ is 1. This gives the absolute lower bound, $\hbar\omega_1$, on the value of $\hbar\omega$ for which transitions are allowed,

$$\omega_1 = \omega_0 - (c_{11}/c_{u11})(\omega_0 + \omega_f), \tag{66}$$

which is simply the value of ω_{ul} in the $\|$ direction when the upper band cuts E_F and in the present case has the value 0.026 eV.

$\cosh v_{\text{lower}}$ is determined by the condition $\omega_l < 0$,

$$\cosh v_{\text{lower}} = \left\{ \frac{\omega_f + (c_{l1}/c_1)(\omega_0 - \omega)}{[(c_{l1}/c_1) + (c_{l11}/c_{11})](\omega_0 - \omega)} \right\}^{1/2}. \tag{67}$$

The absolute lower limit on $\cosh v_{\text{lower}}$ is 1. This occurs for

$$\omega_2 = \omega_0 - (c_{11}/c_{l11})\omega_f, \tag{68}$$

which is the value of frequency for which the lower band cuts E_F in the $\|$ direction. For $\hbar\omega$ greater than this value, 0.12 eV in the present case, transitions are not allowed in a region about L that starts in the $\|$ direction and increases in angle toward the $\perp$ direction as ω increases.

Thus for $\omega \leq \omega_0$, we have $\eta(\omega)$ evaluated from (64). For $\omega < \omega_1$ given by (66), $\eta(\omega)$ is 0. For $\omega_1 < \omega < \omega_2$, we have $\cosh v_{\text{upper}}$ given by (65) and $\cosh v_{\text{lower}}$ by (67). For $\omega_2 < \omega < \omega_0$, we have $\cosh v_{\text{upper}}$ given by (65) and $\cosh v_{\text{lower}} = 1$.

For $\omega_{ul} > \omega_0$, we again evaluate $\eta(\omega)$ by use of a

transformation similar to Eq. (20), but of a form taking account of the fact that the energy difference surfaces are hyperboloids of one sheet.[24] This gives (for $\omega>\omega_0$)

$$\eta(\omega)=(2\pi/c_\perp)[(\omega-\omega_0)/c_{l\parallel}]^{1/2} \times(\sinh u_{\text{upper}}-\sinh u_{\text{lower}}), \quad (69)$$

with $\sinh u_{\text{upper}}$ determined by the condition $\omega_u>0$.

$$\sinh u_{\text{upper}}=\left\{\frac{\omega_0+\omega_f+(c_{u\perp}/c_\perp)(\omega-\omega_0)}{[(c_{u\parallel}/c_{l\parallel})-(c_{u\perp}/c_\perp)](\omega-\omega_0)}\right\}^{1/2}. \quad (70)$$

While $\sinh u_{\text{lower}}$ is determined by the condition $\omega_l<0$,

$$\sinh u_{\text{lower}}=\left\{\frac{\omega_f-(c_{l\perp}/c_\perp)(\omega-\omega_0)}{[(c_{l\parallel}/c_{l\parallel})+(c_{l\perp}/c_\perp)](\omega-\omega_0)}\right\}^{1/2}, \quad (71)$$

where $\sinh u_{\text{lower}}$ is 0 for $\omega>\omega_3$;

$$\omega_3=\omega_0+(c_\perp/c_{l\perp})\omega_f. \quad (72)$$

For $\omega>\omega_3$, 0.55 eV in the present case, the lower band is below E_F in the $\perp$ direction, and optical transitions can occur in the $\perp$ direction.

Thus, to summarize the behavior as a function of frequency of the region about L in which optical transitions are allowed: For $\omega<\omega_1$, there are no transitions allowed anywhere. For $\omega>\omega_1$, transitions are allowed in an angular region about L that starts in the $\parallel$ direction and spreads toward the $\perp$ direction as ω increases. However, at ω_2, the transitions are no longer allowed in the $\parallel$ direction. Thus, for $\omega_2<\omega<\omega_3$, the allowed region extends between two angular limits, both of which are intermediate between the $\perp$ and $\parallel$ directions and both of which are moving toward the $\perp$ direction. At ω_3, transitions become allowed in the $\perp$ direction, and thereafter the region of allowed transitions shrinks in angle steadily toward the $\perp$ direction.

There is the restriction, however, that the upper limit on $\sinh u$ given by (70) can be used only so long as it falls within the maximum volume in k space that can be associated with the neighborhood of a given L point. This maximum volume amounts to $\frac{1}{4}$ of that for the entire Brillouin zone. When the upper limit given by (70) is such as to violate this restriction, it is necessary to use an alternate cutoff on the angular integration in u. The method for doing this is discussed in Ref. 17. It turns out that for the parameters at hand, (70) gives the correct upper limit on $\sinh u$ throughout the frequency range of interest here.

Then $\epsilon_m^{(1)}$ for the $\downarrow$ bands of Model 2 is obtained from (62), including an additional factor of 4 to account for the effect of the four L's in the Brillouin zone, combined with (64), (65), and (67) for $\omega<\omega_0$ and combined with (69), (70), and (71) for $\omega>\omega_0$, using the values of band parameters and Q given in Sec. 3.A. The resulting spectral dependence of $\epsilon_m^{(1)}$ is shown in Fig. 5. It can be seen that the main peak in $\epsilon_m^{(1)}$ occurs at very low frequencies (0.05 eV). The small subsidiary peak at $\hbar\omega_3=0.55$ eV represents a sort of angular critical-point effect as transitions become allowed in the $\perp$ direction.

C. Model 2 $\uparrow$ Bands

For the $\uparrow$ bands, the expressions for ω_u and ω_l are taken the same as (54) and (57) for the $\downarrow$ bands. However, for the $\uparrow$ bands,

$$m_{l\perp}=m_{\perp\uparrow}(L_{32\text{ h.m.}})=\infty. \quad (73)$$

Thus $c_{l\perp}=0$, and $c_\perp=c_{u\perp}$ for the $\uparrow$ bands. The other masses are defined analogously to the $\downarrow$-band case.

$$m_{u\perp}=m_{\perp\uparrow}(L_{2'}), \quad m_{u\parallel}=m_{\parallel\uparrow}(L_{2'}), \quad (74)$$

$$m_{l\parallel}=m_{\parallel\uparrow}(L_{32}). \quad (75)$$

Then $\epsilon_m^{(1)}$ is given by (62) and (69), the same formulas as hold for the $\downarrow$ bands when $\omega>\omega_0$. Here $\sinh u_{\text{lower}}$, determined by the condition $\omega_l<0$, is 0; while for $\omega>|\omega_f|$, we have $\sinh u_{\text{upper}}$ given by (70) with $c_{u\perp}/c_\perp=1$. For $\omega\leq|\omega_f|$, the quantities $\sinh u_{\text{upper}}$ and $\epsilon_{m\uparrow}^{(1)}$ are 0.

Just as for the $\downarrow$ bands, there is the restriction that the upper limit on $\sinh u$ given by (70) applies only so long as it corresponds to values of $k_\perp$ falling within the maximum volume in k space that can be associated with the neighborhood of a given L. Just as for the $\downarrow$ bands, however, for the frequencies of interest here this imposes no additional restriction, so that Eq. (70) applies.

We obtain $\epsilon_m^{(1)}$ for the $\uparrow$ bands of Model 2 from (62) and (69) using the values of parameters given in Sec. 3.A. It is important to note that for corresponding transitions, $\epsilon_m^{(1)}$ for $\uparrow$ and $\downarrow$ bands are opposite in sign. Thus within the framework of our approximation of evaluating $\epsilon_m^{(1)}$ by taking Q as the value at L, the net $\epsilon_m^{(1)}$ is the difference of $\epsilon_{m\downarrow}^{(1)}$ and $\epsilon_{m\uparrow}^{(1)}$. Thus, according to the theory, the onset of $\uparrow$-band transitions appears as a "step" in the total curve for $\epsilon_m^{(1)}$.

4. MODELS 3A AND 3B

In this section, we briefly discuss the derivation of Models 3A and 3B of II, at the same time correcting a numerical error in II. The purpose of II was to illustrate the use of the FKE as a tool for developing models of the band structure of ferromagnetic metals.

In II, the band structure for ferromagnetic nickel was obtained by rigidly splitting the bands of Hanus[21] for nonmagnetic nickel. The band curvatures for the $L_{2'}$ bands ($\uparrow$ and $\downarrow$) were assumed given by the de Haas–van Alphen masses,[22] while the L_{32} band curvatures were found by fitting Hanus' bands as in Sec. 2. The $\downarrow$ bands were placed relative to E_F by choosing the value of onset frequency for the $\epsilon_m^{(1)}$ structure and adopting the model of Sec. 2 for discussing this structure. Then the value of onset frequency together with the band curvatures and separations at L is sufficient to determine $\hbar\omega_0$ of Fig. 3 where $\hbar\omega_0=E_\downarrow(L_{32})-E_F$. Because of uncertainty in the proper way to subtract off the

free carrier-like part of $\epsilon_m^{(1)}$ from the experimental values to get the experimental interband contribution to $\epsilon_m^{(1)}$, two values of onset frequency were chosen, giving rise to Models 3A and 3B, respectively.

Once $E_\downarrow(L_{32})-E_F$ was found, E_p was determined from Eq. (44) of Sec. 2 above by requiring that Q have the value necessary to give the peak value of $\epsilon_m^{(1)}$ obtained experimentally. This value of E_p was used to place the $\uparrow$ bands relative to E_F; while at the same time, fixing Q for the completely defined $\downarrow$-band structure was sufficient to determine $\epsilon_m^{(1)}$ for the $\downarrow$ bands by the methods of Sec. 2 above.

The $\uparrow$ bands for Models 3A and 3B were placed relative to E_F by the use of $\mathbf{k}\cdot\mathbf{p}$ perturbation theory, including nonparabolic effects and the experimental neck radius.[22,27] From $\mathbf{k}\cdot\mathbf{p}$ theory, with $\Delta E=E_F-E_\uparrow(L_{2'})$,

$$\Delta E=-\frac{E_g}{2}+\frac{\gamma\hbar^2k^2_{\text{neck}}}{2m}+\frac{E_g}{2}\left(1+8\frac{\hbar^2k^2_{\text{neck}}}{2m}\frac{E_p}{E_g^2}\right)^{1/2}, \quad (76)$$

where

$$E_g=E(L_{2'})-E(L_{32})=0.08 \text{ eV} \quad (77)$$

for Hanus' bands.

$$\hbar^2k^2_{\text{neck}}/2m=0.03 \text{ eV} \quad (78)$$

from experiment,[22] and

$$\gamma=1+\{2E_p/[E(L_{2'})-E(L_{31})]\}. \quad (79)$$

Once ΔE is determined, thereby placing the $\uparrow$ bands relative to E_F, $\epsilon_m^{(1)}$ for the $\uparrow$ bands is calculated exactly as in Sec. 3.C above.

Unfortunately, a factor of 2 was omitted from Eq. (44) for Q when this was used to evaluate E_p in II. Therefore, the correct value of E_p for Models 3A and 3B is half that used in II. This does not affect the $\downarrow$-band structure or $\epsilon_m^{(1)}$ for the $\downarrow$ bands. However, this does decrease ΔE. This serves to reduce the exchange splitting from 1.15 to 0.89 eV for Model 3A and from 0.77 to 0.61 eV for Model 3B; while the onset frequency for the $\uparrow$-band "step" is reduced from 0.83 to 0.57 eV for Model 3A and from 0.57 to 0.41 eV for Model 3B. The correct spectral variation of $\epsilon_m^{(1)}$ for the two models is shown in Fig. 7.

As indicated above, the reason for treating two models in II was the uncertainty in the proper way to treat the free-carrier-like contribution to $\epsilon_m^{(1)}$ at low frequencies. Doniach has discussed this problem.[6,28] He has considered the contribution to the frequency dependent conductivity of the mechanisms treated by Karplus and Luttinger[29] and by Smit[30] for the dc extraordinary Hall effect. Doniach has then shown that the effects to be expected from these mechanisms can be represented by including a phenomenological tensor force proportional to $\mathbf{M}_s\times\mathbf{E}$ in the classical Drude equation of motion for the free electrons. Unfortunately, there is uncertainty in the appropriate relaxation time[6] to be used in Doniach's theory, and the theory also does not seem to give sufficiently rapid fall-off with increasing frequency of the free-carrier-like contribution to $\epsilon_m^{(1)}$. Thus, at present, the appropriate way to subtract off the free-carrier-like effects from the experimental $\epsilon_m^{(1)}$ to get the experimental interband contribution to $\epsilon_m^{(1)}$ is still not clear.

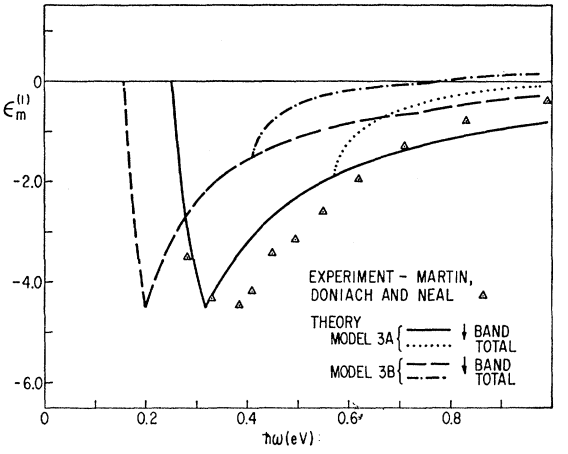

FIG. 7. Spectral dependence of $\epsilon_m^{(1)}$ for Models 3A and 3B.

5. DISCUSSION

In Secs. 2 and 3, we have presented calculations for the interband structure to be expected in the ferromagnetic Kerr effect at low frequencies for each of two models recently proposed for the band structure and Fermi surface of ferromagnetic nickel. As we have indicated above, the calculations discussed here, although containing a number of fairly crude approximations, are absolute, i.e., they contain no adjustable parameters. Much of the uncertainty in the calculation of $\epsilon_m^{(1)}$ stems from the fact that the calculation must relay on a detailed knowledge of the wave functions. While the sign of either the $\uparrow$- or the $\downarrow$-band contribution to $\epsilon_m^{(0)}$ is not determined, the fact that the two contributions are opposite in sign is a requirement of the present theory, independent of any numerical approximations.

It is worthwhile to make a few remarks comparing the results of the two models to each other and to experiment. Model 1 yields structure in $\epsilon_m^{(1)}$ which, on the whole, agrees reasonably well with the experimental results. However, the model of EPO,[7] to which Model 1 corresponds, has a value of d splitting that seems to be unreasonably large in the light of present theories.[31] Despite the fact that the EPO model overestimates the

[27] E. Fawcett and W. A. Reed, Phys. Rev. Letters **9**, 336 (1962).
[28] S. Doniach (unpublished).
[29] R. Karplus and J. M. Luttinger, Phys. Rev. **95**, 1154 (1954).
[30] J. Smit, Physica **24**, 39 (1958).
[31] C. Herring (to be published).

d-band splitting, the Fermi level is determined correctly. This is so, because as long as the lower $d\downarrow$ band is completely filled, the position of the Fermi level is independent of the splitting. Thus the $\downarrow$-band contribution of $\epsilon_m^{(1)}$ for Model 1 is independent of the d-band splitting. On the other hand, Model 2, which corresponds to the model of Phillips and Mattheiss,[8,9] while it has what is probably a more reasonable value for the exchange splitting, shifts the structure in $\epsilon_m^{(1)}$ to very low frequencies. Actually, as can be seen from Figs. 2 and 6, there is not much difference between the $\downarrow$-band structures for the models of EPO and Phillips and Mattheiss. The difference in the structure in $\epsilon_m^{(1)}$ for the two cases comes from the fact that the d bands are so flat that a small shift in energy of the d bands relative to E_F may make a significant change in the amount of k space in which transitions between two bands is allowed. Thus it is not unreasonable to expect that the best model for the band structure of ferromagnetic nickel may be one that maintains a $\downarrow$-band structure with geometry relative to the Fermi energy like that of EPO while having an exchange splitting similar to that of Phillips and Mattheiss. Actually, the estimate of the magneton number given in II for the model of Phillips and Mattheiss is lower than the experimental value, and, as indicated there, this value would also be improved by raising $E_\downarrow(L_{32})$ relative to E_F by 0.1 or 0.2 eV.

Finally, we can make a few remarks regarding the structure to be expected coming from $\uparrow$-band transitions. As indicated above, $\epsilon_m^{(1)}$ from $\uparrow$-band transitions is opposite in sign to that from $\downarrow$-band transitions, and the onset of $\epsilon_m^{(1)}$ for $\uparrow$ bands should appear as a "step" in the measured $\epsilon_m^{(1)}$ curve. Moreover, this "step" should appear at an energy approximately equal to $E_F-E_\uparrow(L_{32})$. Since the main structure from $\downarrow$-band transitions for an EPO-like $\downarrow$-band model occurs at an energy approximately equal to $E_\downarrow(L_{32})-E_F$, the experimental observation of such a "step" in the $\epsilon_m^{(1)}$ curve would directly give the value of the d-band exchange splitting in nickel. While such a "step" might be obscured by broadening effects, the importance of investigating this point experimentally with the greatest possible accuracy seems particularly worth emphasizing. In recent experiments,[5,32] Krinchik has reported that the 0.3-eV peak in $\epsilon_m^{(1)}$ for nickel actually is split into two peaks with a splitting of about 0.05 eV. Krinchik,[32] following the suggestion of Phillips,[9] has attributed this additional structure to spin-orbit splitting of the L_{32} level. On the other hand, an examination of the data of Martin, Doniach, and Neal[6] suggests that while additional structure may be present near the main peak in $\epsilon_m^{(1)}$, it may consist of something more closely resembling the sort of "step" we have described rather than any splitting of the peak. In any case, there is still considerable experimental discrepancy between the data of Krinchik and that of Martin, Doniach, and Neal over the whole range of frequencies investigated, as well as on this particular point. Considering the importance of the information that could be obtained, it would be most valuable for the experiments to be repeated with the greatest possible accuracy in the hope of removing the remaining ambiguity in the experimental results.

ACKNOWLEDGMENTS

The author is grateful to Professor H. Ehrenreich who interested him in this problem and from whose aid and encouragement he benefited during the course of this work. The author wishes to thank Dr. G. S. Krinchik and Dr. D. H. Martin for useful discussions of their experimental data.

[32] G. S. Krinchik, in Proceedings of the International Conference on Magnetism, Nottingham, England, September 1964 (to be published).